Nature Environment and Pollution Technology
An International Quarterly Scientific Journal

p-ISSN: 0972-6268
(Print copies up to 2016)
e-ISSN: 2395-3454

Vol. 22 | No. 1 | pp. 261-268 | 2023

Original Research Paper

https://doi.org/10.46488/NEPT.2023.v22i01.025

Open Access Journal

Utilization of *Enterobacter cloacae* WW1 Biomass for Biosorption of Lead(II) from Aqueous Solution

S. Thongkrua† and A. Kasuya
School of Energy and Environment, University of Phayao, Phayao, Thailand
†Corresponding author: S. Thongkrua; suchanya_9@yahoo.com

Nat. Env. & Poll. Tech.
Website: www.neptjournal.com

Received: 27-06-2022
Revised: 01-08-2022
Accepted: 03-08-2022

Key Words:
Enterobacter cloacae
Bioremediation
Lead-resistant bacteria
Heavy metal

ABSTRACT

The present study evaluated lead biosorption by *Enterobacter cloacae* WW1 isolated from tannery wastewaters under different initial Pb^{2+} concentrations, biomass concentrations, and contact times. The results showed that at an initial Pb^{2+} concentration of 80 $mg.L^{-1}$, the optimal conditions for living cells were a biomass concentration of 7 $g.L^{-1}$ and a contact time of 120 min. For non-living cells, biomass was a biomass concentration of 4 $g.L^{-1}$ and contact time of 45 min, which provided removal efficiencies of 92.03 ± 0.10% and 99.51 ± 0.01%, respectively. The maximum biosorption capacity obtained for non-living cells using an initial Pb^{2+} concentration of 640 $mg.L^{-1}$ was 76.65 ± 0.05 $mg.g^{-1}$. The equilibrium data followed the Langmuir and Freundlich models for living cells, and the data for non-living cell biosorbents fit the Langmuir model. The biosorption kinetics for living and non-living cells fit well with a pseudo-second-order kinetic equation. SEM-EDX analysis clearly showed the morphology and presence of Pb^{2+} particles on non-living cell surfaces after biosorption. In addition, the results revealed that functional groups such as hydroxyl, amino, carboxyl, amide, and phosphate groups on the bacterial cell surface detected by FTIR were associated with the binding of Pb^{2+} ions. The results indicated that *E. cloacae* WW1, a lead-resistant bacterium, can be used as an alternative biosorbent for lead removal from wastewater.

INTRODUCTION

Lead pollution poses major environmental concerns. The significant sources of lead waste are industries such as battery manufacturing, refining, metal plating, smelting, and painting. Lead in the Pb^{2+} state, and its associated hydroxyl compounds are stable, and these are the most prominent forms of lead in nature (Sevak et al. 2021). Discharging Pb-contaminated wastewater into aquatic bodies without treatment can cause many significant environmental problems for aquatic ecosystems and human health (Elgarahy et al. 2021).

Biosorption using a biosorbent based on bacterial biomass to remove heavy metals from wastewater is considered a promising alternative technology owing to the process's high efficacy, low cost, and eco-friendly nature. Lead biosorption by Pb-tolerant bacteria has been studied. These bacteria include gram-positive bacteria, such as *Bacillus badius*, *Bacillus pumilus*, *Lactobacillus brevis*, *Microbacterium oxydans*, *Rhodococcus* sp. and *Lactobacillus acidophilus* (Vishan et al. 2017, Sahoo & Goli 2018, Dai et al. 2019, Afraz et al. 2020), as well as gram-negative bacteria, such as *Klebsiella pneumoniae*, *Staphylococcus* sp., *Pseudomonas* sp. (Li et al. 2017, Aslam et al. 2020, Zhang & Huang 2020, Canaza et al. 2021). Zhang and Huang (2020) reported that the Pb^{2+} biosorption rate using *Shinella zoogloeoides* PQ7 increased from 27.48% to 97.99% when the biomass dosage changed from 0.5 $g.L^{-1}$ to 4.0 $g.L^{-1}$. Canaza et al. (2021) studied Pb^{2+} biosorption by dead biomass of *Pseudomonas monteilii* MA-4. Maximum removal was 250 ppm of Pb(II) within the first 30 min at the biomass of 1 $g.L^{-1}$ and pH of 4. The equilibrium data followed Langmuir and Freundlich isotherm, with q_{max} and K_f values of 166.67 $mg.g^{-1}$ and 11.09, respectively. *Enterobacter cloacae*, lead-resistant bacteria, are gram-negative, rod-shaped, and facultatively anaerobic bacteria (Bhar et al. 2021). Gram-negative bacteria are surrounded by an outer lipid membrane containing lipopolysaccharide and a thin peptidoglycan layer (Thomas et al. 2010). Various functional groups on the bacterial cell wall are known to be involved in heavy metal biosorption (Mitra et al. 2021).

The lead biosorption process depends on many factors, such as the capacity characteristics of the biosorbent, the properties of lead, and environmental conditions. This study aims to investigate Pb^{2+} biosorption by living and non-living *E. cloacae* WW1 biomass isolated from tannery wastewater at varying initial Pb^{2+} concentrations at different biomass concentrations and contact times. Biosorption isotherms and kinetics are also determined.

MATERIALS AND METHODS

Preparation of Bacterial Biomass

E. cloacae WW1, a local lead-tolerant bacterium, was isolated from tannery wastewater in Thailand (Kasuya 2017). *E. cloacae* WW1 was grown in a nutrient broth medium containing 5.0 g beef extract, 2.5 g peptone, 0.1 g potassium nitrate, 2.5 g sodium chloride, and 1 L distilled water and was cultivated in a shaking incubator at 150 rpm and 30°C for 24 h. Bacterial suspensions containing both living and non-living cells obtained by autoclaving at 121°C and 15 Ibs for 30 min were harvested by centrifugation at 8,000 rpm for 20 min. The biomass was rinsed with sterilized distilled water three times and dried at 80°C before the experiment.

Biosorption Experiments

The effects of different initial Pb^{2+} concentrations (40, 80, 160, 320, and 640 $mg.L^{-1}$), biomass concentrations (1, 4, 7, 10, and 13 $g.L^{-1}$), and contact times (5, 10, 15, 20, 25, 30, 45, 60, 120, 240, 360 and 480 min) on the removal efficiency and biosorption capacity of Pb^{2+} were investigated. All experiments were conducted at the laboratory scale with a batch process and were performed in triplicate. A stock solution of Pb^{2+} was prepared using lead(II)acetate $(CH_3COO)_2Pb.Pb(OH)_2$ (Ajax Finechem, Australia). The biomass of living and non-living cells was resuspended in a 150 ml Pb^{2+} solution at an initial pH of 5 and shaken at 120 rpm at room temperature. Then, the suspension was centrifuged at 8,000 rpm for 20 min. The residual Pb^{2+} concentration in the supernatant was analyzed by atomic absorption spectrophotometry (Shimadzu, AA-6880). The surface characteristics of non-living cells before and after biosorption were detected by scanning electron microscopy and energy dispersive x-ray spectroscopy (SEM/EDX), performed with a JEOL JSM-5910LV instrument. In addition, Fourier transforms infrared spectroscopy (FTIR) was also carried out to determine the functional groups presented in non-living cells using a Thermo Scientific spectrometer (model: Nicolet iS5). Discs were prepared by mixing dry samples with a KBr mass ratio of 1:99 (W/W) in an agate mortar and then pressing the sample pellets under a pressure of 7-8 $tons.cm^{-2}$. The FTIR spectra were recorded between 4,000 and 400 cm^{-1} (Bai et al. 2014). The removal efficiency and biosorption capacity of Pb^{2+} were deduced using Eqs. (1) and (2), respectively:

$$Removal\ efficiency\ (\%) = \frac{C_0 - C_t}{C_0} \times 100 \quad \ldots(1)$$

$$q_e = \frac{C_0 - C_e}{M} \times V \quad \ldots(2)$$

Where C_0 ($mg.L^{-1}$) and C_t ($mg.L^{-1}$) are the initial and final Pb^{2+} concentrations, respectively, q_e ($mg.g^{-1}$) and C_e ($mg.L^{-1}$) represent the biosorption capacity and the residual Pb^{2+} concentration at equilibrium, respectively and V (L) and M (g) are the volume of the suspension and the dry biomass in the suspension, respectively (Dai et al. 2019, Canaza et al. 2021).

The biosorption isotherms of Pb^{2+} were analyzed by Langmuir and Freundlich isotherms, which are described in linear forms by Eqs. (3) and (4), respectively:

$$\frac{C_e}{q_e} = \frac{1}{K_L q_m} + \frac{C_e}{q_m} \quad \ldots(3)$$

$$lnq_e = lnK_F + \frac{1}{n} lnC_e \quad \ldots(4)$$

Where q_m ($mg.g^{-1}$) is the maximum specific uptake and K_L represents the Langmuir constant, which relates to the affinity of the binding sites. K_F is defined as the adsorption capacity for Freundlich isotherm, while the adsorption intensity is represented by n (Fathollahi et al. 2021).

The biosorption kinetics of Pb^{2+} were studied using three models, a pseudo-first-order kinetic model, a pseudo-second-order kinetic model, and an intraparticle diffusion model, which can be expressed in linear form as Eqs. (5), (6), and (7), respectively:

$$log(q_e - q_t) = logq_{ecal} - \frac{k_1}{2.303} t \quad \ldots(5)$$

$$\frac{t}{q_t} = \frac{1}{k2^2 qecal^2} + \frac{1}{q_e} t \quad \ldots(6)$$

$$q_t = k_i t^{1/2} + C \quad \ldots(7)$$

where q_t ($mg.g^{-1}$) represents the biosorption capacity at any time t (min), k_1 (min^{-1}), k_2 ($g.mg^{-1}.min^{-1}$), and k_i ($mg.g^{-1}.min^{-1/2}$) are the rate constants for the pseudo-first-order kinetic model, pseudo-second-order kinetic model, and intraparticle diffusion model, respectively, and C ($mg.g^{-1}$) is the constant of diffusion boundary layer thickness (Fathollahi et al. 2021).

RESULTS AND DISCUSSION

Effect of Initial Pb^{2+} Concentration

Fig. 1(a) shows the effect of the initial Pb^{2+} concentration on Pb^{2+} biosorption utilizing *E. cloacae* WW1 with an equilibrium time of 120 min for living cells and 45 min for non-living cells and a biomass concentration of 7 $g.L^{-1}$. For initial Pb^{2+} concentrations from 40 to 640 $mg.L^{-1}$, the extent of Pb^{2+} removal efficiency and biosorption capacity of non-living cells were greater than those of living cells. Since dead bacterial biomass is less sensitive to the toxicity of Pb^{2+}, biosorption may not be inhibited by its presence. The maximum percent removal by living and non-living cells was 92.14 ± 0.05% and 98.54 ± 0.03%, respectively.

The results demonstrated that the removal efficiencies of both biomasses were inhibited at high Pb^{2+} concentrations. Various functional groups, such as carboxyl, amino, hydroxyl, carbonyl, and phosphate groups, are located on the cell walls of bacteria involved in Pb^{2+} biosorption. Some of these groups carry negative changes and bind with Pb^{2+} ions (Tiquia-Arashiro 2018, Mitra et al. 2021). The binding sites on the cell surface became saturated as the initial Pb^{2+} concentration increased. In addition, toxic effects on living cells increase with increasing Pb^{2+} concentrations (Rahman & Singh 2014). The same behavior for Pb^{2+} biosorption (Zhang & Huang 2020) and other heavy metal biosorption (Rahman & Singh 2014) has been reported in previous studies.

On the other hand, the highest biosorption capacities for living and non-living biosorbents achieved at an initial Pb^{2+} concentration of 640 $mg.L^{-1}$ were 59.59 ± 0.01 $mg.g^{-1}$ and 76.65 ± 0.05 $mg.g^{-1}$, respectively. The biosorption capacities of both biosorbents increase with increasing initial Pb^{2+} concentration (Dai et al. 2019). The initial Pb^{2+} concentration regulates the biosorption capacity of Pb^{2+} on the cell surface. This is due to increased free Pb^{2+} ions competing for the available binding sites at greater Pb^{2+} concentrations (Li et al. 2017, Dai et al. 2019, Zhang & Huang 2020).

Effect of Biomass Concentration

A Pb^{2+} biosorption study under different biomass concentrations from 1 to 13 $g.L^{-1}$ was performed in a Pb^{2+} solution of 80 $mg.L^{-1}$, as presented in Fig. 1(b). The results indicated that the Pb^{2+} removal efficiency increased when the biomass concentration increased from 1 to 7 $g.L^{-1}$ for living cells and from 1 to 4 $g.L^{-1}$ for non-living cells. The maximum removal efficiency of living and non-living cells was 92.03 ±0.10% and 97.51±0.01%, respectively. Bacterial surface properties, such as the charge and orientation of the Pb^{2+} binding functional groups on the cell surface, can influence Pb^{2+} biosorption. At higher biosorbent dosages, high surface areas provided large contact areas or a more significant number of binding sites interacting with Pb^{2+} in an aqueous solution (Sethuraman & Balasubramanian 2010). A relevant observation for Pb^{2+} biosorption was presented by Hu et al. (2020) and Zhang and Huang (2020). Moreover, at a high biomass dosage, the removal efficiency was affected by the overlap or aggregation of biosorption sites, resulting in a reduction in the total biosorbent surface available for Pb^{2+} ion binding (Dai et al. 2019, Zhang & Huang 2020). The maximum biosorption capacities of living and non-living cells were achieved at the lowest biomass concentrations of 60.05 ± 0.06 $mg.g^{-1}$ and 64.05 ± 0.06 $mg.g^{-1}$, respectively. These results clearly indicated that the Pb^{2+} biosorption capacity of living and non-living cells decreased with increasing biosorbent concentrations (Sethuraman & Balasubramanian 2010, Li et al. 2017, Dai et al. 2019, Hu et al. 2020, Zhang & Huang 2020). At a high biosorbent dosage, the available Pb^{2+} ions insufficiently covered the binding sites on the biosorbent surface, resulting in a low Pb^{2+} biosorption capacity (Sethuraman & Balasubramanian 2010, Zhang & Huang 2020).

Effect of Contact Time

The influence of contact time (5-480 min) on Pb^{2+} biosorption was studied using a biomass dosage of 7 $g.L^{-1}$ for living cells and 4 $g.L^{-1}$ for non-living cells, as demonstrated in Fig. 1(c). The result showed that the Pb^{2+} elimination percentage for all biomasses increased rapidly in the early stages and then slowed until equilibrium was reached at 120 min for living cells and 45 min for non-living cells due to complexation and binding site saturation on the biosorbent surface (Huang et al. 2013, Li et al. 2017, Zhang & Huang 2020). At equilibrium, the biosorption efficiency and biosorption capacity of living cells were 92.03 ± 0.10% and 10.52 ± 0.01 $mg.g^{-1}$, respectively, and those of non-living cells were 99.51 ± 0.01% and 19.90 ± 0.00 $mg.g^{-1}$, respectively. A similar observation for Pb^{2+} biosorption was reported at an optimal time of 90 min for *Shinella zoogloeoides* PQ7 (Zhang & Huang 2020) and 30 min for *Pseudomonas monteilii* MA-4 (Canaza et al. 2021).

Biosorption Isotherms

The biosorption isotherms of Pb^{2+} on *E. cloacae* WW1 were predicted using Langmuir and Freundlich isotherms. The Langmuir and Freundlich equations are shown in Figs. 2(a) and 2(b), respectively. Table 1 shows the isotherm parameters for Pb^{2+} biosorption. For living cells biosorbents, both the Langmuir and Freundlich models fit well with R^2 values greater than 0.98, which indicates that Pb^{2+} biosorption is a complex surface binding process (Muñoz et al. 2015, Li et al. 2017, Zhang & Huang 2020). For the Freundlich isotherm, an n value > 1 illustrated that Pb^{2+} biosorption was favorable under optimum conditions (Fathollahi et al. 2021).

In contrast, for non-living cells, the experimental data appeared to fit the Langmuir model with an R^2 of 0.9711. This implied that the biosorption of Pb^{2+} occurred at specific homogeneous sites on the biomass surface with monolayer biosorption. Similar results for Pb^{2+} removal from aqueous solutions using *Pseudomonas* sp. I3 was reported by Li et al. (2017). In addition, the value of R_L indicated the shape of the Langmuir isotherm and the nature of the biosorption process, which are expressed in Eq. (8):

$$R_L = \frac{1}{1 + K_L C_0} \quad \ldots(8)$$

The R_L values of living and non-living cells fell within the range of $0 < R_L < 1$, which satisfied the favorable biosorption condition (Yahya et al. 2012). The predicted maximum biosorption capacity (q_m) and K_L for non-living cells were higher than those of living cells. This finding revealed that the non-living biomass was more efficient at adsorbing Pb^{2+} than the living biomass (Huang et al. 2013).

Biosorption Kinetics

The kinetics of Pb^{2+} biosorption onto the living cells and non-living cells of *E. cloacae* WW1 were studied by modeling the data with pseudo-first-order kinetic, pseudo-second-order kinetic, and intraparticle diffusion equations as shown in Fig. 3(a), Fig. 3(b) and Fig. 3(c), respectively. Table 2 presents the kinetics parameters for Pb^{2+} biosorption under the optimum conditions. The pseudo-second-order kinetic model for living and non-living cells had the highest linear correlation coefficients (R^2) of 0.9975 and 0.9998, respectively. The results gave the best fit for the experimental data of all biosorbents. The experimental q_e values were closer to the q_{ecal} values in the pseudo-second-order kinetic model (Zhang & Huang 2020). Furthermore, the rate constant

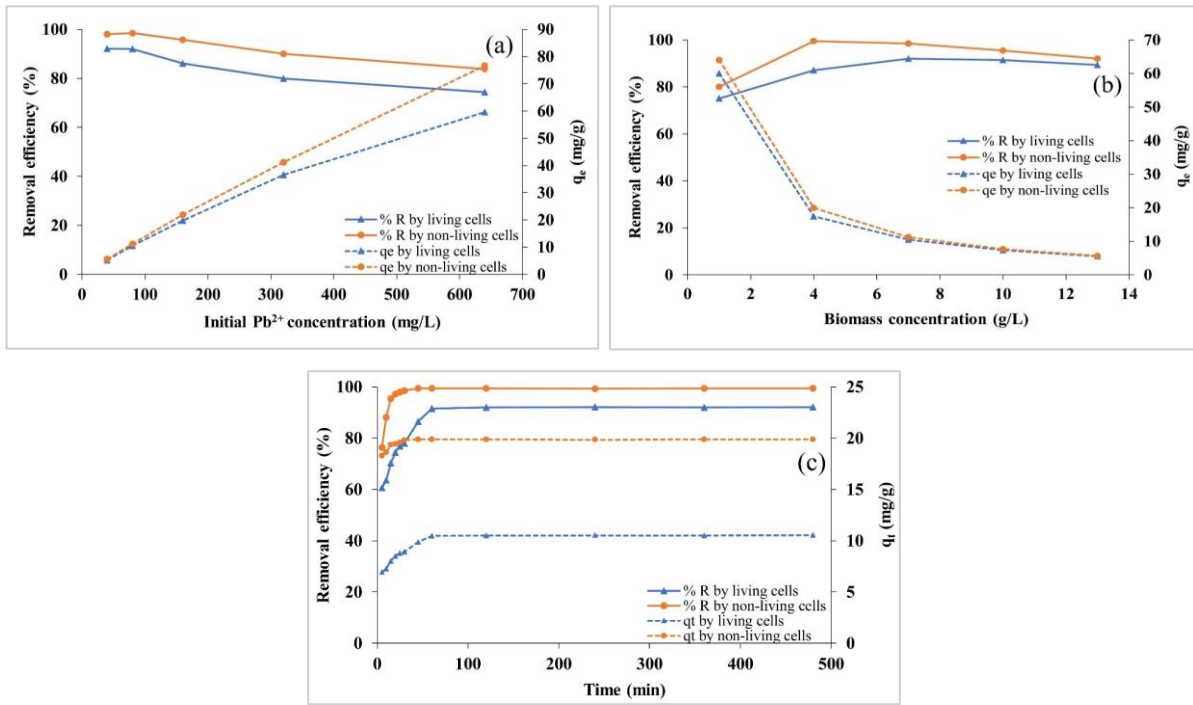

Fig. 1: The effect of the initial Pb^{2+} concentration (a), biomass concentration (b), and contact time (c) on Pb^{2+} biosorption.

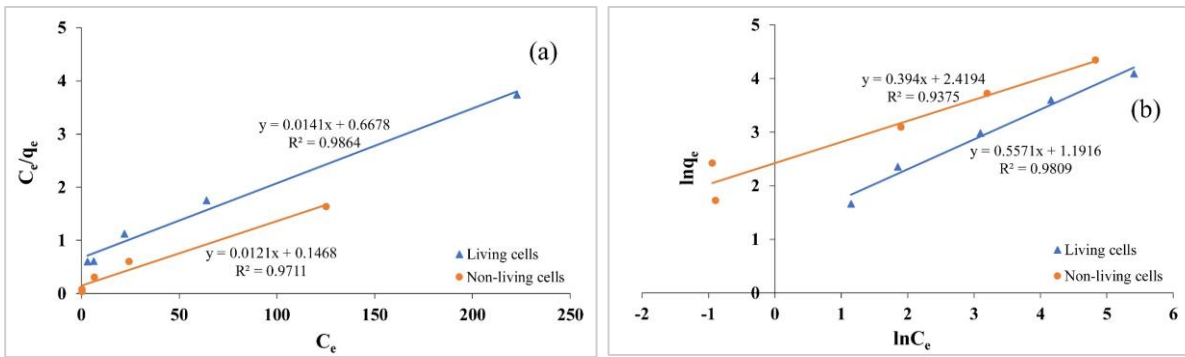

Fig. 2: Langmuir (a) and Freundlich (b) isotherm for Pb^{2+} biosorption.

Table 1: Isotherm parameters for Pb^{2+} biosorption.

Biosorbents	Langmuir isotherm				Freundlich isotherm		
	q_m [mg.g^{-1}]	k_L [L.mg^{-1}]	R_L	R^2	n	k_F	R^2
Living cells	70.92	0.02	0.07	0.9864	1.80	3.29	0.9809
Non-living cells	82.64	0.08	0.02	0.9711	2.54	11.24	0.9375

of k illustrated that the Pb^{2+} biosorption of non-living cells was faster than that of living cells (Huang et al. 2013). In addition, it was also observed that the intraparticle plot did not pass through the origin, which indicated that intraparticle diffusion is not the sole process involved in biosorption. The results revealed that Pb^{2+} biosorption was a chemisorption process involving Pb^{2+} binding to the cell surface (Muñoz et al. 2015, Zhang & Huang 2020). According to a relevant study, Pb^{2+} biosorption kinetics were found to fit well with pseudo-second-order kinetic models for gram-negative bacteria (Muñoz et al. 2015, Li et al. 2017, Zhang & Huang 2020) and gram-positive bacteria such as *Bacillus* spp. (Vishan et al. 2017, Cai et al. 2018, Mohapatra et al. 2019).

SEM and EDX Analysis

The morphological characterization and EDX spectra of non-living cells of *E. cloacae* WW1 before and after Pb^{2+} biosorption (80 mg.L^{-1}) are shown in Fig. 4. Fig. 4(a) illustrates that before biosorption, the non-living cells biosorbents were rod-shaped with clear boundaries (Song et al. 2017, Zhang et al. 2019, Dash et al. 2021). The EDX spectra shown in Fig. 4(c) recorded signals for carbon, nitrogen, oxygen, and phosphorus as present in the polysaccharides and proteins of biomass and did not show a Pb^{2+} signal (Ghosh et al. 2022). The presence of lower amounts of oxygen and a high amount of carbon indicate that the non-living cells were more effective biosorbents for metal removal from aqueous solutions (Biswas et al. 2019). After biosorption, the Pb^{2+} particles adhered to the cell surface after 45 min, as depicted in Fig. 4(b). Similarly, selenium (Se) aggregates onto the cell surface of *E. cloacae* Z0206 (Song et al. 2017), and the surface of *E. cloacae* RSN3 becomes rough after arsenic (As) uptake (Dash et al. 2021). Furthermore, the EDX spectra shown in Fig. 4(d) revealed that Pb^{2+} accumulated on the surface of non-living cells (Muñoz et al. 2015, Hasan et al. 2016, Jalilvand et al. 2020).

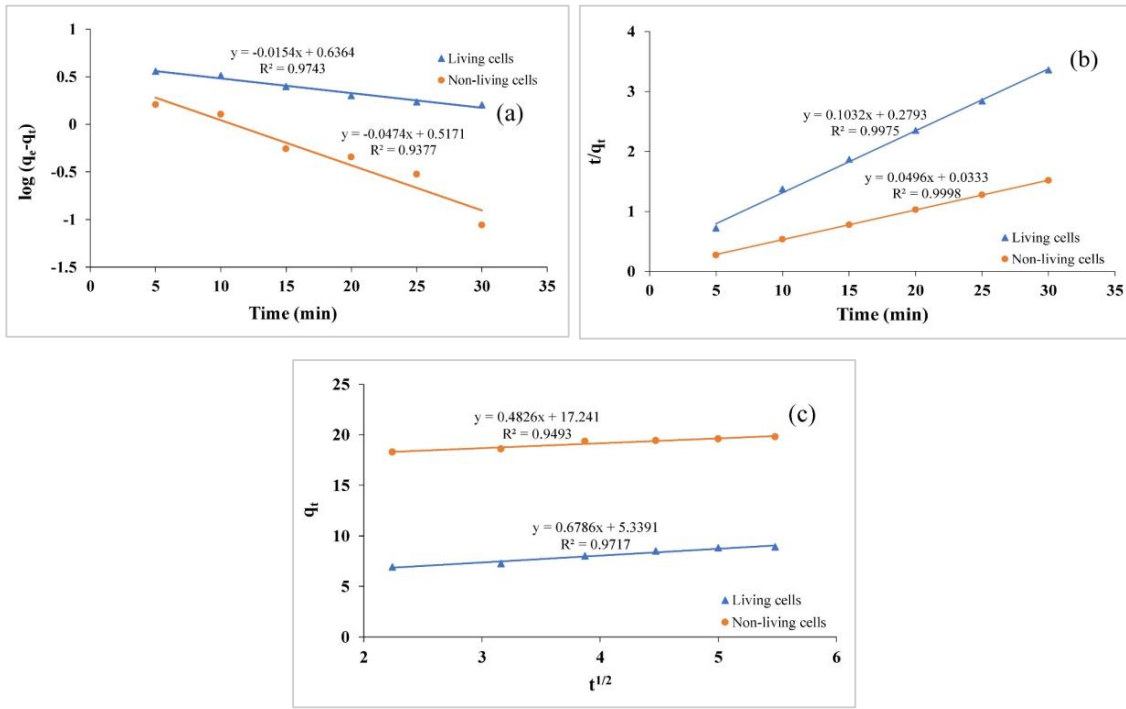

Fig. 3: Pseudo-first-order kinetic (a), Pseudo-second-order kinetic (b), and Intraparticle diffusion (c) model for Pb^{2+} biosorption.

Table 2: Kinetic model parameters for Pb^{2+} biosorption.

Biosorbents	Pseudo-first-order kinetic model			Pseudo-second-order kinetic model			Intraparticle diffusion model		
	q_{ecal} [$mg.g^{-1}$]	k_1 [min^{-1}]	R^2	q_{ecal} [$mg.g^{-1}$]	k_2 [$g.mg^{-1}.min^{-1}$]	R^2	k_i [$mg.g^{-1}.min^{-1/2}$]	C [$mg.g^{-1}$]	R^2
Living cells	4.33	0.04	0.9743	9.69	0.20	0.9975	0.68	5.34	0.9717
Non-living cells	3.29	0.11	0.9377	20.16	0.27	0.9998	0.48	17.24	0.9493

FTIR Analysis

FTIR analysis of non-living *E.cloacae* WW1 cells before and after Pb^{2+} biosorption was carried out to confirm the presence of functional groups on the cell surface responsible for the biosorption process (Fig. 5). Fig. 5(a) shows the FTIR spectrum for Pb^{2+} preadsorption. The broad peak in the range of 3367.59-3484.74 cm^{-1} was assigned to the stretching of O-H groups in polysaccharides (Ghosh et al. 2022). The transmission spectrum at approximately 3350.71 cm^{-1} was attributed to proteins' amino groups (N-H). Another peak ranging from 2913.43-2962.13 cm^{-1} indicated C-H bonds in alkyl groups in proteins and carbohydrates of the cell wall (Suriya et al. 2013, Bai et al. 2014, Ghosh et al. 2022). A sharp peak at 1652.70 cm^{-1} represented the stretching vibrations of carboxyl groups (C=O) (Hasan et al. 2016,

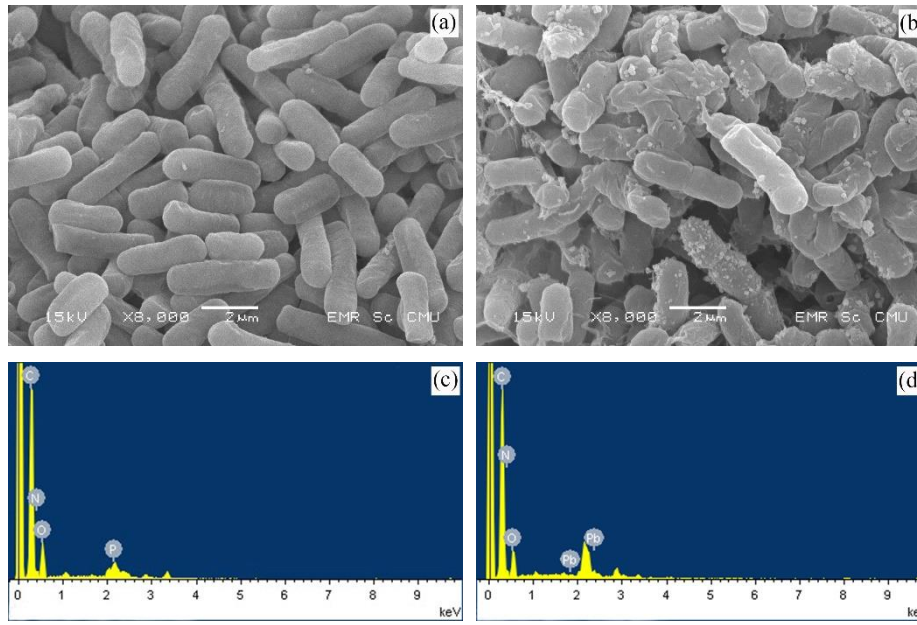

Fig. 4: SEM micrographs and EDX spectra of non-living cells of *E. cloacae* WW1 before biosorption (a and c) and after biosorption (b and d).

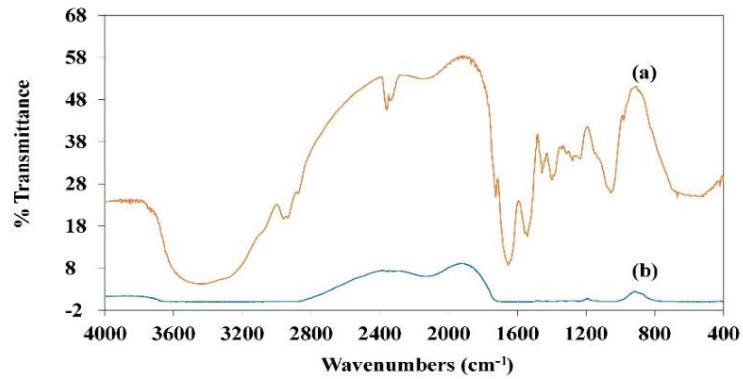

Fig. 5: FTIR spectra of the non-living cells of *E. cloacae* WW1 before biosorption (a) and after biosorption (b).

Ghosh et al. 2022). The bands approximately 1645.46 and 1573.15 cm^{-1} corresponded to amide I and amide II, respectively (Suriya et al. 2013, Bai et al. 2014). The peak observed approximately 1055.35 cm^{-1} denoted phosphate groups (Muñoz et al. 2015, Zhang & Huang 2020). The hydroxyl, amino, carboxyl, amide, and phosphate groups presented on the cell surface participate in the binding of Pb^{2+} ions (Tiquia-Arashiro 2018). After the biosorbent was exposed to Pb^{2+}, several functional group spectra were shifted and decreased in band intensity, such as the phosphate groups in polysaccharides (1040.89 cm^{-1}) (Fig. 5(b)). The results revealed that functional groups on the bacterial cell surface were associated with Pb^{2+} biosorption (Muñoz et al. 2015, Zhang & Huang 2020). Similar results were observed for cadmium (Ghosh et al. 2022) and copper biosorption (Suriya et al. 2013) using *E. cloacae*.

CONCLUSION

E. cloacae WW1 isolated from tannery wastewaters was used to explore Pb^{2+} biosorption at varying initial Pb^{2+} concentrations, biomass concentrations, and contact times. The Pb^{2+} removal efficiency and biosorption capacity of non-living cells were higher than those of living cells. Because dead bacterial biomass is insensitive to lead toxicity, its biosorption is independent of metabolism. The maximum percent removal obtained from non-living cells was 99.51±0.01% under an initial Pb^{2+} concentration of 80 $mg.L^{-1}$, a biomass concentration of 4 $g.L^{-1,}$ and a contact time of 45 min. Furthermore, non-living cells also showed the highest biosorption capacity of 76.65±0.05 $mg.g^{-1}$ at an initial Pb^{2+} concentration of 640 $mg.L^{-1}$. The biosorption isotherm and kinetic data for non-living cells were consistent with the Langmuir model and a pseudo-second-order kinetic model, respectively. This indicated that Pb^{2+} biosorption occurred at specific homogeneous sites on the biomass surface with monolayer biosorption and consisted of a chemisorption process involving Pb^{2+} binding to the cell surface. The lead-tolerant bacterial strain *E. cloacae* WW1 can be utilized for the biosorption of lead-contaminated waters because of several advantages, such as its rapid and high-efficiency processes, low potential cost, and eco-friendliness.

ACKNOWLEDGEMENT

The authors are grateful to the School of Energy and Environment and the School of Science, University of Phayao, for laboratory equipment support.

REFERENCES

Afraz, V., Younesi, H., Bolandi, M. and Hadiani, M.R. 2020. Optimization of lead and cadmium biosorption by *Lactobacillus acidophilus* using response surface methodology. Biocatal. Agric. Biotechnol., 29: 1-7.

Aslam, F., Yasmin, A. and Sohail, S. 2020. Bioaccumulation of lead, chromium, and nickel by bacteria from three different genera isolated from industrial effluent. Int. Microbiol., 23: 253–261.

Bai, J., Yang, X., Du, R., Chen, Y., Wang, S. and Qiu, R. 2014. Biosorption mechanism involved in immobilization of soil Pb by *Bacillus subtilis* DBM in a multi-metal-contaminated soil. J. Environ. Sci., 26: 2056-2064.

Bhar, S., Edelmann, M.J. and Jones, M.K. 2021. Characterization and proteomic analysis of outer membrane vesicles from a commensal microbe, *Enterobacter cloacae*. J. Proteomics, 231: 103994.

Biswas, R., Vivekanand, V., Saha, A., Ghosh, A. and Sarkar, A. 2019. Arsenite oxidation by a facultative chemolithotrophic *Delftia* spp. Bas29 for its potential application in groundwater arsenic bioremediation. Int. Biodeterior. Biodegrad., 136: 55-62.

Cai, Y., Li, X., Liu, D., Xu, C., Ai, Y., Sun, X., Zhang, M., Gao, Y., Zhang, Y., Yang, T., Wang, J., Wang, L., Li, X. and Yu, H. 2018. A novel Pb-resistant *Bacillus subtilis* bacterium isolate for co-biosorption of hazardous Sb(III) and Pb(II): thermodynamics and application strategy. Int. J. Environ. Res. Pub. Health, 15(4): 1-18.

Canaza, A., Pozo, L., Ferrufino-Guardia, E. and Vargas, V. A. 2021. Biosorption of lead(II) ions by dead bacterial biomass isolated from mine water. Rev. Boliv. Quím., 38(3): 119-125.

Dai, Q.H., Bian, X.Y., Li, R., Jiang, C.B., Ge, J. M., Li, B. L. and Ou, J. 2019. Biosorption of lead(II) from aqueous solution by lactic acid bacteria. Water Sci. Technol., 79(4): 627-634.

Dash, B., Sahu, N., Singh, A. K., Gupta, S. B. and Soni, R. 2021. Arsenic efflux in *Enterobacter cloacae RSN3* isolated from arsenic-rich soil. Folia Microbiol., 66: 189-196.

Elgarahy, A.M., Elwakeel, K.Z., Mohammad, S.H. and Elshoubaky, G.A. 2021. A critical review of biosorption of dyes, heavy metals and metalloids from wastewater as an efficient and green process. Clean. Eng. Technol., 4: 1-15.

Fathollahi, A., Coupe, S.J., El-Sheikh, A.H. and Nnadi, E.O. 2021. Cu(II) biosorption by living biofilms: isotherm, chemical, physical and biological evaluation. J. Environ. Manage., 282: 1-13.

Ghosh, A., Pramanik, K., Bhattacharya, S., Mondal, S., Ghosh, S.K. and Maiti, T.K. 2022. A potent cadmium bioaccumulating *Enterobacter cloacae* strain displays phytobeneficial property in Cd-exposed rice seedlings. Curr. Res. Microb. Sci., 3: 1-14.

Hasan, H.A., Abdullah, S.R.S., Kofli, T. and Yeoh, S. J. 2016. Interaction of environmental factors on simultaneous biosorption of lead and manganese ions by locally isolated *Bacillus cereus*. J. Ind. Eng. Chem., 37: 295-305.

Hu, X., Cao, J., Yang, H., Li, D., Qiao, Y., Zhao, J., Zhang, Z. and Huang, L. 2020. Pb^{2+} biosorption from aqueous solutions by live and dead biosorbents of the hydrocarbon-degrading strain *Rhodococcus* sp. HX-2. PLOS ONE, 15(1): 1-24.

Huang, F., Dang, Z., Guo, C.-L., Lu, G.-N., Gu, R. R., Liu, H.J. and Zhang, H. 2013. Biosorption of Cd (II) by live and dead cells of *Bacillus cereus* RC-1 isolated from cadmium-contaminated soil. Coll. Surf. B Biointerf., 107: 11-18.

Jalilvand, N., Akhgar, A., Alikhani, H.A., Rahmani, H.A. and Rejali, F. 2020. Removal of heavy metals zinc, lead, and cadmium by biomineralization of urease-producing bacteria isolated from Iranian mine calcareous soil. J. Soil Sci. Plant Nutr., 20: 206-219.

Kasuya, A. 2017. Treatment of Lead in Synthetic Wastewater by Biosorption. Thesis, University of Phayao, Thailand.

Li, D., Xu, X., Yu, H. and Han, X. 2017. Characterization of Pb^{2+} biosorption by psychrotrophic strain *Pseudomonas* sp. I3 isolated from permafrost soil of Mohe wetland in Northeast China. J. Environ. Manage., 196(1): 8-15.

Mitra, A., Chatterjee, S., Kataki, S., Rastogi, R.P. and Gupta, D.K. 2021. Bacterial tolerance strategies against lead toxicity and their relevance in bioremediation application. Environ. Sci. Pollut. Res., 28: 14271–14284.

Mohapatra, R.K., Parhi, P.K., Pandey, S., Bindhani, B.K., Thatoi, H. and Panda, C.R. 2019. Active and passive biosorption of Pb(II) using live and dead biomass of marine bacterium *Bacillus xiamenensis* PbRPSD202: kinetics and isotherm studies. J. Environ. Manage., 247: 121-134.

Muñoz, A.J., Espínola, F., Moya, M. and Ruiz, E. 2015. Biosorption of Pb(II) ions by *Klebsiella* sp. 3S1 isolated from a wastewater treatment plant: kinetics and mechanisms studies. Biomed. Res. Int., 2015: 1-12.

Rahman, Z. and Singh, V.P. 2014. Cr (VI) reduction by *Enterobacter* sp. DU17 isolated from the tannery waste dump site and characterization of the bacterium and the Cr (VI) reductase. Int. Biodeterior. Biodegradation, 91: 97-103.

Sahoo, S. and Goli, D. 2018. Bioremediation of lead by a halophilic bacteria *Bacillus pumilus* isolated from the mangrove regions of Karnataka. Int. J. Sci. Res., 9(1): 1337-1343.

Sethuraman, P. and Balasubramanian, N. 2010. Removal of Cr(VI) from aqueous solution using *Bacillus subtilis*, *Pseudomonas aeruginosa* and *Enterobacter cloacae*. Int. J. Eng. Sci. Technol., 2(6): 1811-1825.

Sevak, P.I., Pushkar, B.K. and Kapadne, P.N. 2021. Lead pollution and bacterial bioremediation: A review. Environ. Chem. Lett., 19: 4463-4488.

Song, D., Li, X., Cheng, Y., Xiao, X., Lu, Z., Wang, Y. and Wang, F. 2017. Aerobic biogenesis of selenium nanoparticles by *Enterobacter cloacae* Z0206 as a consequence of fumarate reductase mediated selenite reduction. Sci. Rep., 7: 1-10.

Suriya, J., Bharathiraja, S. and Rajasekaran, R. 2013. Biosorption of heavy metals by biomass of *Enterobacter cloacae* isolated from metal-polluted soils. Int. J. ChemTech. Res., 5(3): 1329-1338.

Thomas, J.S., Kahne, D. and Walker, S. 2010. The bacterial cell envelope: Cold spring harb. Perspect. Biol., 2(5): 1-16.

Tiquia-Arashiro, S.M. 2018. Lead absorption mechanisms in bacteria as strategies for lead bioremediation. Appl. Microbiol. Biotechnol., 102: 5437-5444.

Vishan, I., Laha, A. and Kalamdhad, A. 2017. Biosorption of Pb(II) by *Bacillus badius* AK strain originating from rotary drum compost of water hyacinth. Water Sci. Technol., 75(5-6): 1071-1083.

Yahya, S.K., Zakaria, Z.A., Samin, J., Raj, A.S.S. and Ahmad, W.A. 2012. Isotherm kinetics of Cr(III) removal by non-viable cells of *Acinetobacter haemolyticus*. Coll. Surf. B Biointerf., 94: 362-368.

Zhang, W. and Huang, Y. 2020. The synthesis of PbS NPs and biosorption of Pb(II) by *Shinella zoogloeoides* PQ7 in aqueous conditions. Water, 12(7): 1-14.

Zhang, Y., Wang, X., Li, X., Dong, L., Hu, X., Nie, T., Lu, Y., Lu, X., Pang, J., Li, G., Yang, X., Li, C. and You, X. 2019. Synergistic effect of colistin combined with PFK-158 against colistin-resistant *Enterobacteriaceae*. Antimicrob. Agents Chemother., 63(7): 1-10.